REPORT DOCUMENTATION PAGE

Form Approved OMB NO. 0704-0188

1. REPORT DATE (DD-MM-YYYY)	2. REPORT TYPE	3. DATES COVERED (From - To)
23-02-2016	Final Report	1-Oct-2010 - 30-Sep-2013

4. TITLE AND SUBTITLE
Final Report: Advanced Research in Optical Refrigeration and Applications (ARORA)

5a. CONTRACT NUMBER
W911NF-10-1-0499

5b. GRANT NUMBER

5c. PROGRAM ELEMENT NUMBER
0620BJ

6. AUTHORS
Mansoor Sheik-Bahae

5d. PROJECT NUMBER

5e. TASK NUMBER

5f. WORK UNIT NUMBER

7. PERFORMING ORGANIZATION NAMES AND ADDRESSES
University of New Mexico Albuquerque
1700 Lomas Blvd. NE, Suite 2200, MSC01 1247
1 University of New Mexico
Albuquerque, NM 87131 -0001

8. PERFORMING ORGANIZATION REPORT NUMBER

9. SPONSORING/MONITORING AGENCY NAME(S) AND ADDRESS (ES)
U.S. Army Research Office
P.O. Box 12211
Research Triangle Park, NC 27709-2211

10. SPONSOR/MONITOR'S ACRONYM(S)
ARO

11. SPONSOR/MONITOR'S REPORT NUMBER(S)
58848-PH-DRP.12

12. DISTRIBUTION AVAILIBILITY STATEMENT
Approved for Public Release; Distribution Unlimited

13. SUPPLEMENTARY NOTES
The views, opinions and/or findings contained in this report are those of the author(s) and should not contrued as an official Department of the Army position, policy or decision, unless so designated by other documentation.

14. ABSTRACT
A significant improvement in thermal properties is measured for the sapphire thermal link, compared to the fused silica link. When measured quantitatively, it can be seen that no thermal barrier exists for the Van Der Waals bonded sapphire link, while adhesive imposes significant impedance. Additionally, no thermal gradient exists along the length of the sapphire link, thanks to the high thermal conductivity, whereas the fused silica link exhibits a significant gradient.

15. SUBJECT TERMS
Optical Refrigeration, Yb:YLF crystal cooling

16. SECURITY CLASSIFICATION OF:			17. LIMITATION OF ABSTRACT	15. NUMBER OF PAGES	19a. NAME OF RESPONSIBLE PERSON
a. REPORT	b. ABSTRACT	c. THIS PAGE			Mansoor Sheik-Bahae
UU	UU	UU	UU		19b. TELEPHONE NUMBER 505-277-2080

Report Title

Final Report: Advanced Research in Optical Refrigeration and Applications (ARORA)

ABSTRACT

A significant improvement in thermal properties is measured for the sapphire thermal link, compared to the fused silica link. When measured quantitatively, it can be seen that no thermal barrier exists for the Van Der Waals bonded sapphire link, while adhesive imposes significant impedance. Additionally, no thermal gradient exists along the length of the sapphire link, thanks to the high thermal conductivity, whereas the fused silica link exhibits a significant gradient.

Enter List of papers submitted or published that acknowledge ARO support from the start of the project to the date of this printing. List the papers, including journal references, in the following categories:

(a) Papers published in peer-reviewed journals (N/A for none)

Received		Paper
02/02/2016	5.00	Denis V. Seletskiy, Markus P. Hehlen, Richard I. Epstein, Mansoor Sheik-Bahae. Cryogenic optical refrigeration, Advances in Optics and Photonics, (03 2012): 79. doi: 10.1364/AOP.4.000078
02/02/2016	6.00	Denis V. Seletskiy, Seth D. Melgaard, Richard I. Epstein, Alberto Di Lieto, Mauro Tonelli, Mansoor Sheik-Bahae. Local laser cooling of Yb:YLF to 110 K, Optics Express, (09 2011): 1. doi: 10.1364/OE.19.018229
02/02/2016	7.00	Mohammadreza Ghasemkhani, Alexander R. Albrecht, Seth D. Melgaard, Denis V. Seletskiy, Jeffrey G. Cederberg, Mansoor Sheik-Bahae. Intra-cavity cryogenic optical refrigeration using high power vertical external-cavity surface-emitting lasers (VECSELs), Optics Express, (06 2014): 16232. doi: 10.1364/OE.22.016232
02/02/2016	9.00	Seth Melgaard, Denis Seletskiy, Victor Polyak, Yemane Asmerom, Mansoor Sheik-Bahae. Identification of parasitic losses in Yb:YLF and prospects for optical refrigeration down to 80K, Optics Express, (03 2014): 7756. doi: 10.1364/OE.22.007756
02/03/2016	10.00	Denis V. Seletskiy, Seth D. Melgaard, Richard I. Epstein, Alberto Di Lieto, Mauro Tonelli, Mansoor Sheik-Bahae. Precise determination of minimum achievable temperature for solid-state optical refrigeration, Journal of Luminescence, (10 2013): 5. doi: 10.1016/j.jlumin.2011.09.045
02/03/2016	11.00	J.G. Cederberg, A.R. Albrecht, M. Ghasemkhani, S.D. Melgaard, M. Sheik-Bahae. Growth and testing of vertical external cavity surface emitting lasers (VECSELs) for intracavity cooling of Yb:YLF, Journal of Crystal Growth, (05 2014): 28. doi: 10.1016/j.jcrysgro.2013.09.042
TOTAL:		**6**

Number of Papers published in peer-reviewed journals:

(b) Papers published in non-peer-reviewed journals (N/A for none)

Received Paper

TOTAL:

Number of Papers published in non peer-reviewed journals:

(c) Presentations

Number of Presentations: 0.00

Non Peer-Reviewed Conference Proceeding publications (other than abstracts):

Received Paper

TOTAL:

Number of Non Peer-Reviewed Conference Proceeding publications (other than abstracts):

Peer-Reviewed Conference Proceeding publications (other than abstracts):

Received	Paper	
02/02/2016	1.00	Alexander R. Albrecht, Mohammadreza Ghasemkhani, Jeffrey G. Cederberg, Denis V. Seletskiy, Seth D. Melgaard, Mansoor Sheik-Bahae, Richard I. Epstein, Denis V. Seletskiy, Mansoor Sheik-Bahae. Progress towards cryogenic temperatures in intra-cavity optical refrigeration using a VECSEL, SPIE OPTO. 02-FEB-15, San Francisco, California, USA. : ,
02/02/2016	2.00	Chengao Wang, Mansoor Sheik-Bahae, Jeffrey Cederberg, Daniel Bender, Richard I. Epstein, Denis V. Seletskiy, Mansoor Sheik-Bahae. Accurate measurement of external quantum efficiency in semiconductors, SPIE OPTO. 02-FEB-13, San Francisco, California, USA. : ,
02/02/2016	3.00	Mansoor Sheik-Bahae, Mohammad Ghasemkhani, Alexander R. Albrecht, Denis V. Seletskiy, Jeffrey G. Cederberg, Seth D. Melgaard, Jennifer E. Hastie. Intracavity-enhanced laser cooling of solids using high power VECSELs at 1020 nm, SPIE LASE. 26-FEB-13, San Francisco, California, USA. : ,
02/02/2016	4.00	Alexander R. Albrecht, Denis V. Seletskiy, Jeffrey G. Cederberg, Alberto Di Lieto, Mauro Tonelli, Jerome V. Moloney, Ganesh Balakrishnan, Mansoor Sheik-Bahae, Richard I. Epstein, Mansoor Sheik-Bahae. Intracavity laser cooling using a VECSEL, SPIE OPTO. 21-JAN-12, San Francisco, California. : ,
02/02/2016	8.00	Richard I. Epstein, Denis V. Seletskiy, Mansoor Sheik-Bahae, Seth D. Melgaard, Denis V. Seletskiy, Richard I. Epstein, Jay V. Alden, Mansoor Sheik-Bahae. Device applications of cryogenic optical refrigeration, SPIE OPTO. 01-FEB-14, San Francisco, California, United States. : ,
TOTAL:	**5**	

Number of Peer-Reviewed Conference Proceeding publications (other than abstracts):

(d) Manuscripts

Received	Paper
TOTAL:	

Number of Manuscripts:

Books

Received Book

TOTAL:

Received Book Chapter

TOTAL:

Patents Submitted

Patents Awarded

Awards

Graduate Students

NAME	PERCENT_SUPPORTED	Discipline
Ghasemkhani	0.22	
Melgaard	0.33	
FTE Equivalent:	**0.55**	
Total Number:	**2**	

Names of Post Doctorates

NAME	PERCENT_SUPPORTED
Albrecht	0.08
FTE Equivalent:	**0.08**
Total Number:	**1**

Names of Faculty Supported

NAME	PERCENT_SUPPORTED	National Academy Member
Sheik-Bahae	0.17	
FTE Equivalent:	**0.17**	
Total Number:	**1**	

Names of Under Graduate students supported

NAME	PERCENT_SUPPORTED
FTE Equivalent:	
Total Number:	

Student Metrics

This section only applies to graduating undergraduates supported by this agreement in this reporting period

The number of undergraduates funded by this agreement who graduated during this period: 0.00

The number of undergraduates funded by this agreement who graduated during this period with a degree in science, mathematics, engineering, or technology fields:..... 0.00

The number of undergraduates funded by your agreement who graduated during this period and will continue to pursue a graduate or Ph.D. degree in science, mathematics, engineering, or technology fields:..... 0.00

Number of graduating undergraduates who achieved a 3.5 GPA to 4.0 (4.0 max scale):..... 0.00

Number of graduating undergraduates funded by a DoD funded Center of Excellence grant for Education, Research and Engineering:..... 0.00

The number of undergraduates funded by your agreement who graduated during this period and intend to work for the Department of Defense 0.00

The number of undergraduates funded by your agreement who graduated during this period and will receive scholarships or fellowships for further studies in science, mathematics, engineering or technology fields: 0.00

Names of Personnel receiving masters degrees

NAME
Total Number:

Names of personnel receiving PHDs

NAME
Total Number:

Names of other research staff

NAME	PERCENT_SUPPORTED
FTE Equivalent:	
Total Number:	

Sub Contractors (DD882)

Inventions (DD882)

Scientific Progress

See attached.

Technology Transfer

N/A

Final Report

Advanced Research in Optical Refrigeration and Applications (ARORA)

PI: Mansoor Sheik-Bahae
Institution: University of New Mexico, Albuquerque, NM
Date: March 18, 2014

I. Experimental demonstration of cooling a Yb:YLF crystal below NIST-defined cryogenic temperature of 123 K.

In our milestone paper (Nature Photonics, 2010), we reported the first cryogenic operation using optical refrigeration in Yb:YLF crystal by cooling to 155 K. We also predicted that the current Yb:YLF crystal is capable of cooling down to ~110 K when pumped at 1020 nm with sufficiently high power. We verified the feasibility of this experiment by developing a novel technique that can measure the minimum achievable temperature (MAT) with high accuracy. In this technique, we place the sample in a cryostat and cool it to a given temperature. We then use a tunable laser (Ti:sapphire) to measure the cooling efficiency spectrum at that temperature. The key experimental technique that enabled this measurement was the development of two-pixel differential luminescence thermometry (2P-DLT), which allowed a rapid measurement of local heating or cooling. The results are summarized in Fig. 1 where the calculated and experimental cooling efficiency are compared. This was presented at Photonics West conference in 2011.

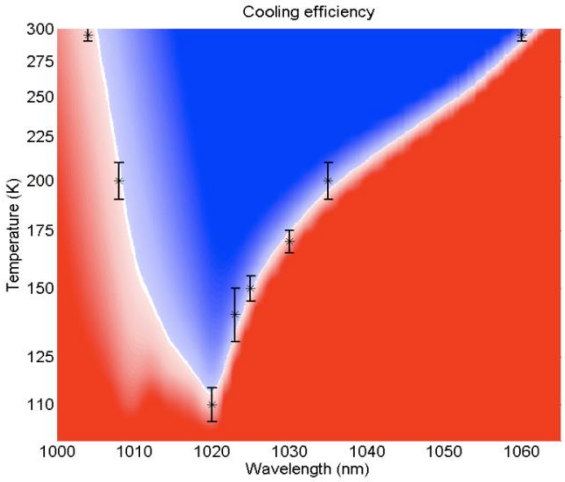

Fig. 1. Cooling efficiency versus temperature and pump laser wavelength calculated from the known spectral data of 5% Yb:YLF. The white border describes transition from cooling (blue) to heating (red) regime. The data points measured using 2P-DLT are shown for comparison.

With the successful verification that our 5% doped Yb:YLF is capable of cooling to 110 K, we needed a high power laser source at 1020 nm to demonstrate cooling to this temperature from room temperature with a respectable cooling power. We purchased a custom-made Yb-fiber laser (from IPG Photonics) with 50W CW power at 1020.8 nm. For the cooling experiments, we set up a table-top vacuum chamber, evacuated to 10^{-6} torr using a turbo-molecular pump to reduce convective heat load on the sample. To minimize conductive heat load, the cooling crystal is supported by short glass fibers. Radiative heat load on the sample is reduced by surrounding it with a clamshell coated with a specialized low thermal emissivity, high optical absorption coating.

Since the absorption in the Yb:YLF sample decreases for lower temperatures, it is not sufficient to direct the pump laser beam through the sample just once. Ideally, almost all of the pump light could be absorbed in the sample using a matched resonant cavity. Unfortunately, instabilities in the pump laser make this technique difficult to implement and we instead opted for a non-resonant cavity as shown in Fig. 2: The Yb:YLF cooling sample is placed between two high-reflecting mirrors, with the laser entering the non-resonant cavity through a small hole in the first mirror. The light then makes several passes (10~20) through the sample and any light not absorbed exits the cavity again through the same hole in the input mirror. This design has proven to be very robust against laser instabilities while still greatly increasing the amount of absorbed light.

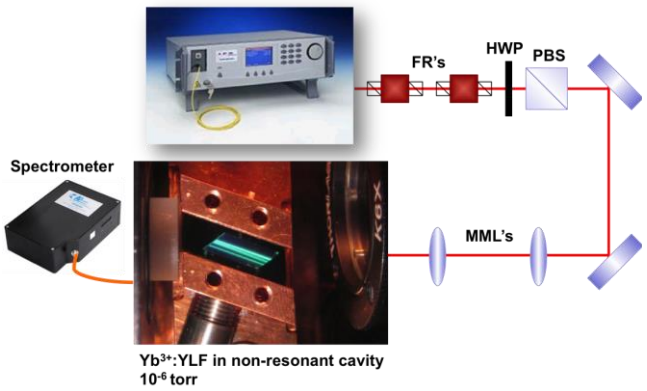

Fig. 2. Schematic diagram of experimental setup using non-resonant cavity for enhanced absorption.

Another area we investigated was the increase of the Yb doping levels in the YLF crystal. In addition to the previously characterized 5% Yb:YLF sample, concentrations of 7% and 10% were investigated as well. From optical measurements, we can extract the cooling efficiency of each sample, plotted as function of the laser wavelength for the different Yb concentrations in Fig. 3(a). By fitting the measured cooling efficiency data points to our laser cooling theory, we can extract the external quantum efficiency, which is essentially identical for all the samples at η_{ext} = (99.6 ± 0.1) % as well as the background absorption, which is shown in Fig. 3(b) as function of the Yb doping concentration. There is a clear trend towards lower background absorption at higher doping levels, with the 10% Yb:YLF sample exhibiting a record-low background absorption of $\alpha_b = 2.0 \times 10^{-4}$ cm^{-1}.

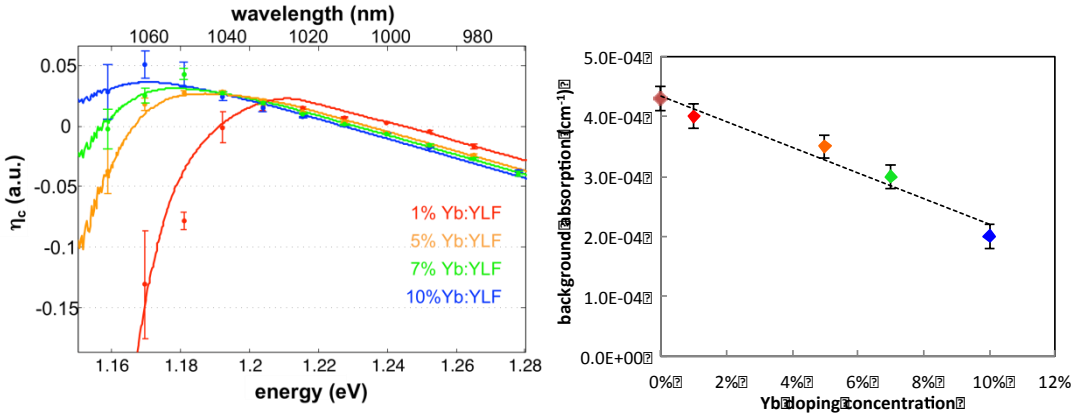

Fig. 3. (a) Measurement and fitting of the cooling efficiency for Yb:YLF samples of variable doping at 300 K, yielding η_{ext} = (99.6 ± 0.1)% and varying background absorption;(b) background absorption coefficient obtained from the fits versus Yb doping concentration.

The low background absorption combined with the increased doping concentration of the 10% sample should result in a dramatic improvement of the cooling performance, which we therefore modeled. Neglecting temperature dependence of η_{ext} and α_b, we calculate the cooling efficiency using measured values of $\eta_{abs}(\lambda, T)$ and η_{ext}. Fig. 4(a) reveals cooling efficiency as a function of wavelength and temperature, along with a MAT of ~ 93 K at ~1020 nm, corresponding to the transition between E4 and E5 levels of the 2F7/2−2F5/2 Stark manifold of Yb^{3+}. This global minimum achievable temperature corresponds to a strong improvement in comparison with the 5% sample. To verify this prediction, we investigated cooling performance in a high power cooling setup as shown in Fig. 2. While currently limited by the pump power trapping efficiency, we nonetheless were able to achieve cooling to an absolute temperature of 114 ± 1 K, starting from ambient, with an estimated cooling power of 750 mW (Fig. 4(b)). This result corresponds to a new low-temperature record for optical refrigeration and indirectly attests to the correctness of the low MAT prediction.

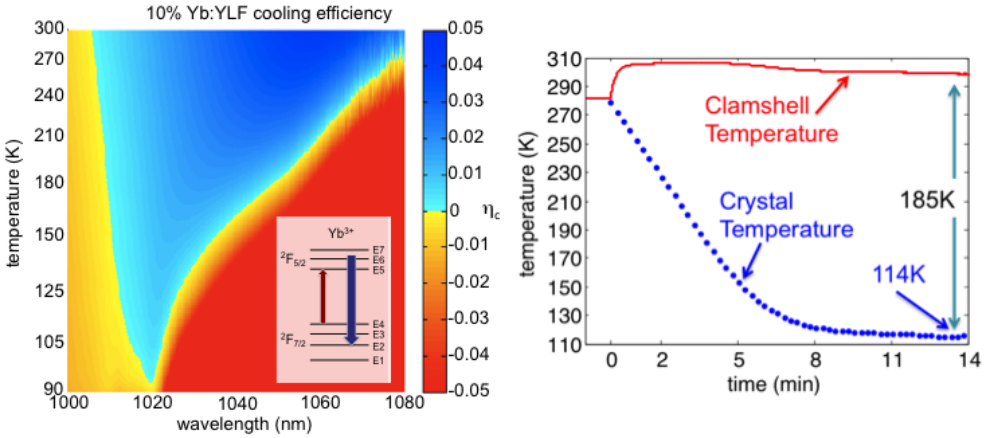

Fig. 4. (a) Cooling efficiency for 10% Yb:YLF sample. Minimum achievable temperature of 93 K is obtained at the E4-E5 transition of Yb^{3+} ion (red vertical arrow on inset); (b) Plot of temperature vs. time for 10% Yb:YLF pumped at 1020nm resulting in 114K ± 1K.

II. Elemental analysis to identify source of background absorption.

Due to the importance and surprising correlation of the background absorption with doping concentration, we turned our attention to an investigation of the nature of the background absorption. Our Yb:YLF crystals are grown from three starting materials: YbF_3, YF_3, and LiF. Scaling of the α_b with doping relies on the exact path by which the impurities can enter the final crystal, during the growth process. For instance, if impurities were introduced through the YbF_3 starting material, increasing the doping concentration would proportionally increase the level of impurities, thus potentially negating the benefit of higher resonant absorption. The observed anti-correlation between background absorption and doping level (Fig. 3(b)) however suggests that we can rule out YbF_3 as the major source of impurities. Furthermore, the anti-correlated behavior of these two quantities suggests that at least some background absorption material is introduced through the YF_3 starting material, which is being substituted by YbF_3 during the growth. Of course, at high concentrations, linear approximation will fail, due to an increased probability of energy transfer between two neighboring Yb^{3+} ions, as the distance between ions decreases. On average this energy transfer alone does not cause unwanted heating, but instead increases the probability for an excitation to reach an impurity where it will decay non-radiatively, causing heat. This is called concentration quenching and sets an upper limit on the doping concentration, which in turn depends on the impurity levels of the material. The observed linear decrease of the background absorption in our samples with increase of the doping concentration (Fig. 3(b)) however suggests the influence of the concentration quenching up to the 10% is not evident. We also note that while the linear decrease of impurities with doping is highly encouraging, laser cooling performance will most likely be detrimentally affected by concentration quenching at doping levels in the 10-20% range. Investigation of laser cooling in such heavily-doped samples is currently underway by our group.

Elemental analysis is an ideal tool to identify the constituent elements that produce parasitic heating and hence to understand the trend in the optical measurements. Sample dissolution and subsequent procedures were carried out in a class 100 cleanroom at the Radiogenic Isotope Laboratory at the University of New Mexico in collaboration with Victor Polyak and Yemane Asmerom. Without a method of dissolution of $LiYF_4$ available in literature, a method was developed for sample preparation, prior to elemental analysis. The crystal is first cleaned with ultra-pure de-ionized water. One of the surfaces is removed and discarded by scraping with a tungsten carbide bit to remove any remaining surface impurities and expose the internal crystal from where the dissolution sample is scraped, taking care to avoid any surface that has not been previously removed. This scraping also serves to finely crush the sample, necessary for dissolution. The systematic dissolution method for Yb:YLF used for this work is as follows: The previously prepared powdered sample is combined with ultra-pure HNO_3 and HCL, covered with a lid and boiled at 120°C for at least 4 hours to drive off the fluorine atoms. The lid is removed and dissolution of the powder is verified visually in the remaining liquid. If completely dissolved, the remaining liquid is evaporated on a hot plate. A solution of 3% HNO_3 with 10 ppb indium (^{115}In) for a dilution of 1:1000, e.g. a15mg of original powder, diluted with 15ml of solution, is added. ^{115}In is an internal standard used by the instrument to monitor any signal suppression or enhancement from the solution matrix and other instrument variability. Blanks (monitor for trace element contribution from reagents; 3% HNO_3 spiked with 10 ppb indium) were run with the samples; given the purity of our reagents, blank correction was not significant.

A Thermo X-series II quadrupole inductively coupled plasma mass spectrometer (Q-ICPMS) was used for the trace elemental analysis. We did an initial semi-quantitative survey followed by 26 elements quantitatively with a concentration range from 1,000 ppt to 100,000 ppt. Elemental standards in the range of the concentration of the elements of interest were used to construct calibration curves. Overall precision ranged from 0.01% to 102% (1σ) including all 26 elements, however by removing ^{82}Se from the set, the precision improved to 0.01% to 17.46% (1σ) and 0.81% to 4.08% (1σ) for Fe. Without a priori knowledge of which impurities cause heating, it is necessary to analyze as many elements as possible to compare to the background absorption measurement obtained from optical experiments.

For a 5-sample set, the full dimensionality of our dataset is 5×N, where N is the number of trace elements analyzed. To reduce dataset to 1×N, we replace the 5-sample column by the correlation coefficient r. This coefficient represents statistical correlation between quantities A and B and lies on the segment [-1;1], where 0 corresponds to the case of no statistical correlation between A and B, while positive/negative extrema correspond to perfect correlation/anti-correlation between these quantities. We plot r for correlation between the Yb^{3+} doping level (top) and background absorption (bottom) in Fig. 5. We first note the nearly perfect correlation ($r \approx 1$) of nominal Yb doping with concentration of ^{172}Yb, which attests to excellent growth calibration as well as great sensitivity of Q-ICPMS. Furthermore, near-unity positive correlation coefficients observed for ^{153}Eu, ^{159}Tb, ^{165}Ho, ^{169}Tm elements imply that they are introduced together with the Yb through the YbF_3 starting material. Additionally, strong anti-correlation ($r < -0.8$) observed for ^{51}V and ^{58}Fe suggests that these elements are displaced during the process of Yb doping, in other words these elements most likely belong to the YF_3 starting material due to the $Y^{3+} \rightarrow Yb^{3+}$ substitution. Here we would like to note that we have chosen to detect ^{58}Fe instead of a naturally abundant ^{56}Fe in order to avoid common isobaric interference in the mass spectrometry of the latter. The concentrations of these two Fe isotopes are related, thus not affecting the drawn conclusions.

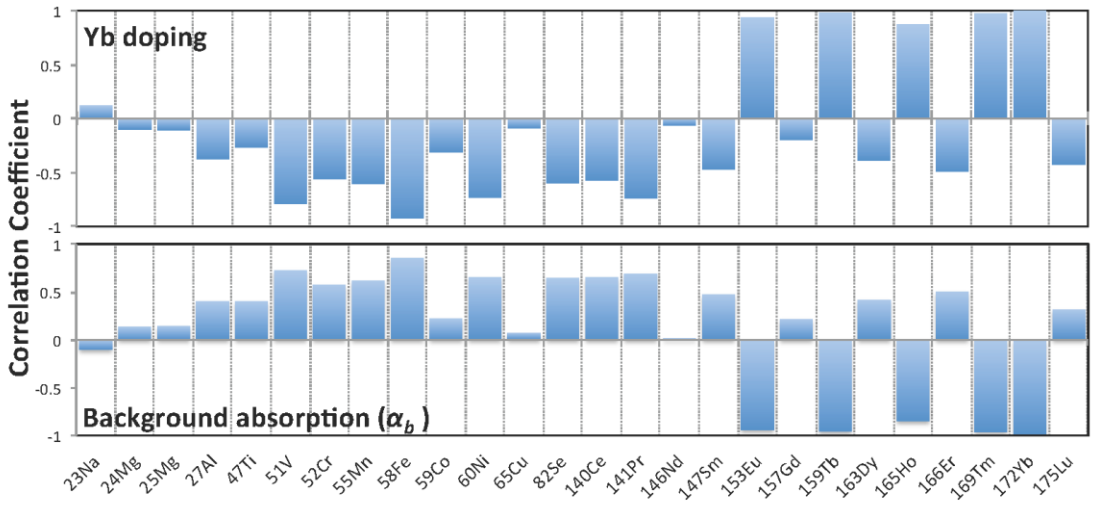

Fig. 5. Statistical correlation of elemental sample composition with Yb doping (top) and background absorption (bottom). Strong correlation of α_b with ^{58}Fe identifies the transition metal as potentially dominant impurity in current optical cryocoolers.

It is remarkable to note that ^{58}Fe exhibits pronounced peak with $r \sim 0.9$ in the correlation with measured background absorption, indicating that the presence of iron is the main source of the background absorption. It should be noted here that further investigation of the oxidation state of Fe is necessary. Previous investigations concerned the oxidation state Fe^{2+} where absorption is strong around 1000 nm corresponding to the mean fluorescence of Yb^{3+}. The oxidation state Fe^{3+} absorbs between 700-850 nm, and hence could still contribute to background absorption, as being resonant with the higher-energy states of Tm^{3+} unintentional co-dopant. In Yb:YLF, charge compensation is necessary to incorporate Fe^{2+}. An electron paramagnetic resonance spectroscopy study is currently underway to verify the oxidation state of Fe in YLF. Combining these findings with the compositional information, we can draw an additional conclusion that iron impurity is most likely introduced through the YF_3 starting material. This is further corroborated by the optical measurements and provides direct feedback to the material synthesis in terms of the potential targets for starting materials purification efforts.

To further support this interpretation, we carried out elemental analysis on an additional 5%-doped Yb:YLF sample, grown in a different laboratory and most probably under different growth conditions. Due to the growth variations, this sample cannot be combined with the original 5-sample set to draw compositional conclusions, as above. Nonetheless, the measured background absorption and concentration of iron are in very good agreement with the trend measured from the controlled sample set (Fig. 6). Here the iron concentration has been scaled by the natural isotope abundance ratio of ^{56}Fe relative to the measured ^{58}Fe in the mass spectrometer. The observed correlation suggests the generality of our finding that the presence of the transition-metal iron in current Yb:YLF cryocoolers limits the performance, by increase in the background absorption and hence the global minimum achievable temperature value. The calculated MAT value of 93 K, as shown in Fig. 4(a) is already a considerable improvement from earlier performance. With an additional factor of 2 reduction of Fe in the YF_3 starting material, operation close to 80 K is calculated, promising a bright future for the next generation optical cryocoolers.

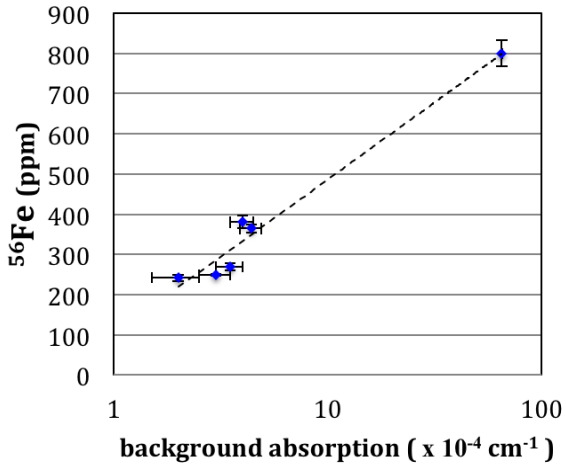

Fig. 6. Iron concentration (in parts per million, ppm) versus optically measured background absorption in six different Yb:YLF samples. The strong correlation points to iron as the main source of parasitic background absorption in currently available optical cryocoolers.

III. Intracavity Cooling Using Optically Pumped Semiconductor Lasers (OPSL).

One of our major goals is to develop and demonstrate concepts for compact and efficient all-solid-state cryocoolers. One concept is based on intra-cavity enhanced cooling using optically pumped semiconductor lasers (OPSL), also called vertical-external-cavity surface-emitting lasers (VECSEL), as schematically shown in Fig. 7.

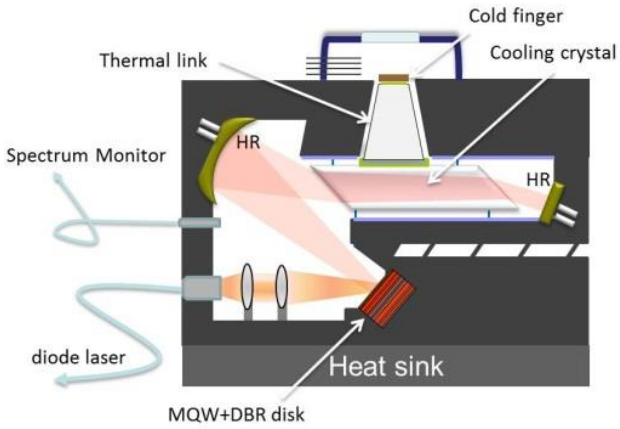

Fig. 7. Intra-Cavity Enhanced Cryogenic Optical REfrigerator (ICE-CORE) based on a diode-pumped semiconductor laser.

Towards this goal, we have a fruitful collaboration with Jeffrey Cederberg at Sandia National Lab (Albuquerque) who is an expert in MOCVD epitaxial growth of III-V semiconductors. We developed 1020 nm high power InGaAs multi-quantum-well (MQW) active regions using GaAsP barrier material for strain compensation and binary GaAs/AlAs distributed Bragg reflectors (DBR) for improved thermal conductivity. The samples are grown in "bottom-emitter" geometry, where the active region is grown on the substrate first, followed by the DBR. The sample is then coated with thin Titanium and Gold layers for adhesion, and a ~2 µm Indium layer, to solder the sample to an equally coated CVD diamond plate heat spreader. A selective wet etch that stops on a InGaP window layer is then used to remove the complete GaAs substrate, leaving only the <10 µm thick VECSEL disc on the heat spreader. This provides excellent cooling for the gain chip and allowed us to reach CW output powers in excess of 20 W as shown in Fig. 8, without any signs of thermal roll-over, only limited by the available pump power.

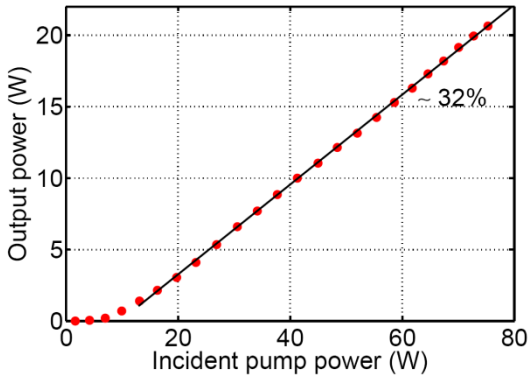

Fig. 8. VECSEL CW output power, using a 5% transmission output coupler, as function of incident pump power.

Control of the output wavelength of the VECSEL is crucial for laser cooling. On reason is to counteract the pump-power-dependent gain shift caused by heating of the VECSEL chip, thus ensuring the possibility of 1020 nm operation, needed to achieve the lowest possible temperature. To accomplish wavelength control of the VECSEL, we employ a 4 mm thick quartz birefringent filter (BF), inserted in the external cavity at Brewster's angle. The BF allows us to tune the VECSEL from 1000 nm to 1030 nm as shown in Fig. 9(a). A home-made scanning Fabry-Perot interferometer is used to measure the full width at half maximum (FWHM) of the VECSEL linewidth to be 0.15±0.02 nm at 1020 nm for 40 W of incident pump power, as shown in Fig. 9(b). This narrow linewidth is ideally matched for pumping of the E4-E5 Yb^{3+} transition.

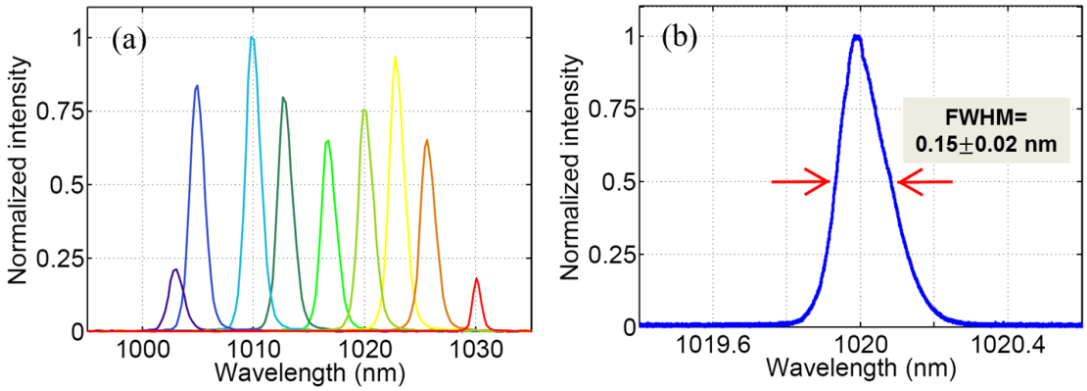

Fig. 9. (a) VECSEL lasing spectra for different orientations of the BF (linewidth is limited by resolution of grating spectrometer); (b) High-resolution scan of VECSEL linewidth via home-built Fabry-Perot interferometer reveals FWHM of 0.15±0.02 nm at 1020 nm.

Another important parameter of interest for laser cooling is the maximum amount of intracavity loss (i.e. absorption of light in the cooling sample) that can be tolerated by the VECSEL. To simulate the variable loss in the cavity, we inserted a fused silica window initially at the Brewster's angle and then incrementally rotated it to introduce increasing reflection losses. The resulting total output power as a function of the roundtrip loss in the cavity is illustrated in Fig. 10 for 40 W of incident pump power. While it is apparent that more than 15 % of roundtrip loss can be overcome by the VECSEL, we determine the optimal roundtrip loss to be approximately 4-5 % for this pumping condition. To optimize power extraction and efficiency, we design the sample for optimal coupling at a wavelength of 1020 nm and low temperatures of Yb:YLF.

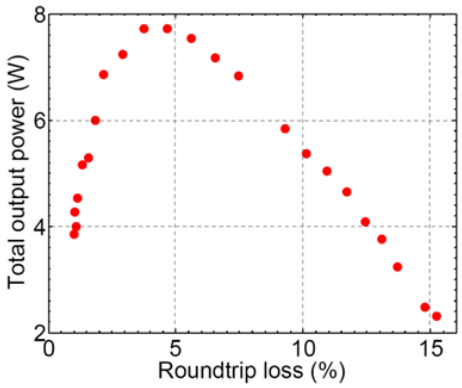

Fig. 10. Total VECSEL output power for 40 W of pump power as a function of roundtrip loss as adjusted by the angle of an intracavity window. The total output power combines the power of reflected beams from the intracavity window and the output power from a 1% output coupler.

For our cooling experiments, we choose a 7% Yb:YLF sample. Assuming a target temperature of 120 K at a wavelength of 1020 nm, this yields a sample thickness of approximately 2 mm for optimal coupling. However, since the absorption coefficient of the cooling sample changes significantly with temperature, as shown in Fig. 11, the exact same Yb:YLF crystal would exhibit an absorption in excess of 35% per round trip at room temperature, significantly too high for the VECSEL to reach threshold. Therefore, at room temperature the VECSEL wavelength is tuned to approximately 1030 nm, where the round-trip loss is estimated to be around 9 %, allowing for the operation of the laser. Once the Yb:YLF starts cooling, we gradually tune the wavelength toward 1020 nm (needed to achieve the lowest possible temperature), such that the absorbed power and roundtrip cavity loss in the crystal is maintained despite the decreasing absorption coefficient.

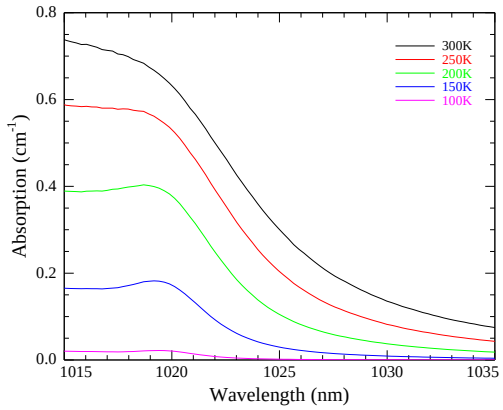

Fig. 11. Absorption coefficient for Yb:YLF for different temperatures.

The laser cooling experiment is conducted in a vacuum chamber, similar to the one used in section I. This time, however, the whole VECSEL cavity is located inside the vacuum, as schematically shown in Fig. 12. The collimated beam from a 75 W fiber coupled 808 nm pump laser outside the vacuum chamber is sent through an anti-reflection (AR) coated vacuum-port window. Two 5 cm and 7.5 cm focal length lenses are used to image the pump laser onto a 300 μm diameter spot on the VECSEL gain chip; any pump light reflected at the semiconductor surface is redirected outside to reduce heating the inside of the vacuum chamber. The external cavity of the VECSEL is comprised of a 20 cm radius of curvature mirror, mounted in a 3-axis piezo-actuated mirror mount for fine tuning of the VECSEL alignment during the cooling experiment. The 4 mm thick birefringent filter for tuning the lasing wavelength is adjusted using a torque cable and rotation feedthrough. The Yb:YLF crystal is inserted in the cavity under Brewster's angle and supported by microscope cover slips (100 μm thick) in order to reduce conductive heat load. Non-contact temperature measurement is accomplished via the technique of differential luminescence thermometry (DLT) for real-time temperature monitoring of the cooling sample. For this purpose fluorescence is collected by a multi-mode optical fiber positioned in the vicinity of the Yb:YLF crystal and fed through a fiber-optic vacuum port to an outside CCD line spectrometer. The temperature of the crystal as function of time is shown in Fig. 13(a). Since the cooling sample is very small, the lowest temperature of 131 K is reached within 5 minutes of starting the experiment. Fig. 13(b) shows examples of the fluorescence spectra used to extract sample temperature. Also visible is some scattered laser light, illustrating the tuning of the wavelength during the experiment, as described above.

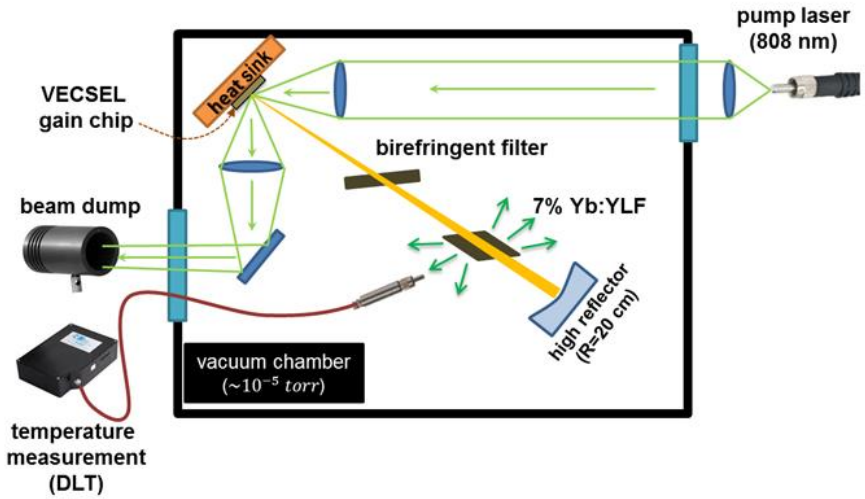

Fig. 12. Schematic diagram of the VECSEL intracavity laser cooling experiment.

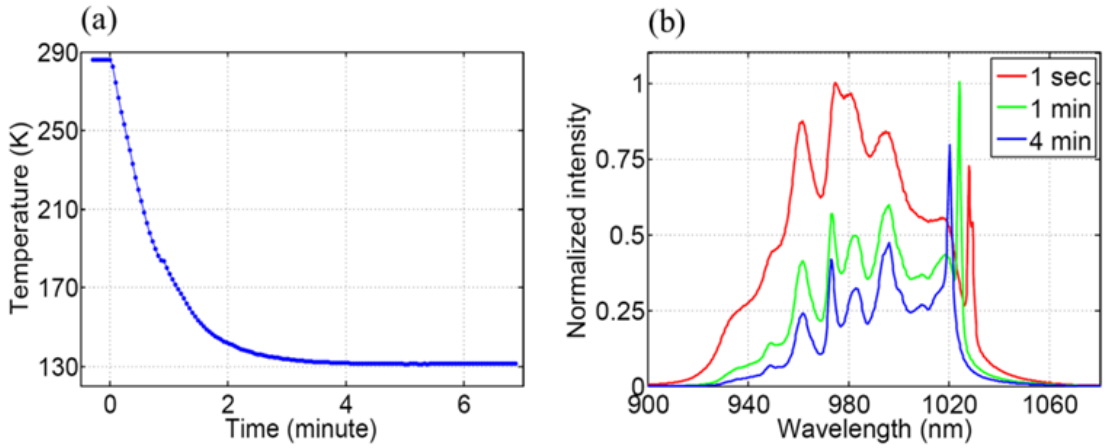

Fig. 13. (a) Yb:YLF crystal temperature as a function of time during cooling experiment. Cooling to 131 K was achieved starting from the room temperature. (b) Normalized luminescence spectra (not corrected for instrument response) at different times; note the scattered intracavity laser light at 1020 nm to 1030 nm.

IV. Thermal Link Design, Fabrication, and Testing.

The purpose of a real laser cooling device is to cool a load, which typically is not transparent to the wavelengths of light involved in the cooling process. Any absorption would therefore lead to heating of the load, counteracting the cooling from the Yb:YLF sample. This is avoided by using a thermal link to optically isolate an applied load from the high power fluorescence generated by the optical refrigeration process, yet still provide a pathway of high thermal conductivity to remove heat from the load. Initial thermal link designs were analyzed with ZEMAX, a ray tracing software, to determine the optical rejection of various thermal link shapes, Fig. 14.

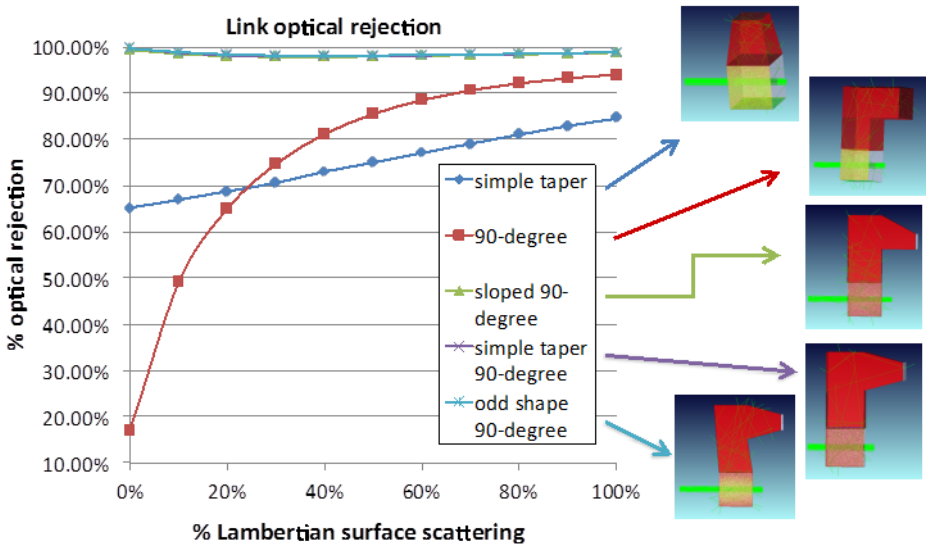

Fig. 14. Plot of optical rejection as a function of lambertian surface scattering with images of the thermal link shapes to the right. Each link is analyzed as a ratio of photons incident on the link end where a load is to be applied with the photons entering the thermal link. As expected, increased link complexity provides increased optical rejection.

As the link complexity increases, the optical rejection improves. In this study, only link shapes, which can be easily fabricated in the lab are considered. However, by increasing the number of "kinks", the link will provide increased optical rejection at the cost of slightly reduced thermal conductivity. Optical rejection should surpass 99% with increased number of kinks. With a modeled understanding of the optical rejection in place, a fused silica link was fabricated to experimentally verify the optical rejection properties prior to implementation of a high thermal conductivity link made of sapphire. The fused silica link is cut and slightly polished, to help ensure cleanliness, from a high quality fused silica window. The size is matched to a 5% Yb:YLF crystal and is bonded to the crystal with a UV curable optical adhesive. At this stage it is understood that the thermal properties will be far from desirable, with a thermal gradient between the cooling crystal, the UV adhesive, and the thermal link as seen in Fig. 15, but it is a necessary step toward understanding the optical properties of the thermal link.

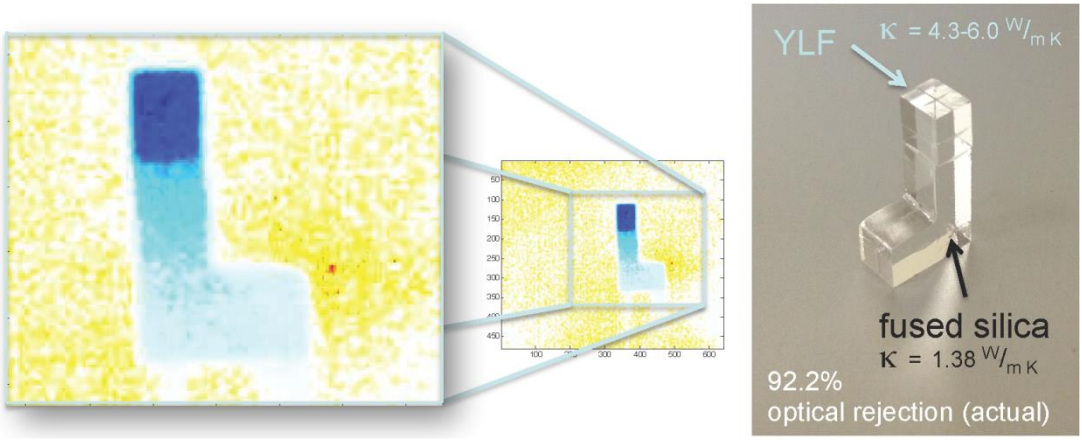

Fig. 15. Thermal image of the fused silica thermal link bonded to a 5% Yb:YLF crystal. Cooling can be seen in the crystal which has been false colored as blue, whit a significant discontinuity at the adhesive interface between cooling crystal and thermal link. Photograph of device.

The optical rejection measurements require precise determination of the fluorescence generated that enters the thermal link, as well as the total fluorescence incident on the thermal link end. Measurements are therefore taken using a large area silicon detector, which closely matches the surface area of each face being analyzed, 3x3 mm^2, coupled with shielding to prevent spurious fluorescence and external sources of light from altering the measurement, as well as index matching fluid between the measured face and the detector to ensure consistent photon counts by removing total internal reflection. Experimental measurements of 92.2% optical rejection match well with ZEMAX models where a simple 90^o kink should provide between 92%-94% optical rejection for the given surface quality.

With models matching experimental measurements of a fused silica link, the next step of fabricating a high conductivity thermal link from sapphire was undertaken, Fig. 16. Two significant improvements are utilized. First, a thermal link is fabricated out of sapphire, which has nearly 30x higher thermal conductivity than fused silica. Second, the thermal link is Van Der Waals bonded to a piece of 10% Yb:YLF crystal, removing the adhesive thermal barrier. The same optical measurements undertaken for the fused silica link are performed for the sapphire link with 92.9% optical rejection.

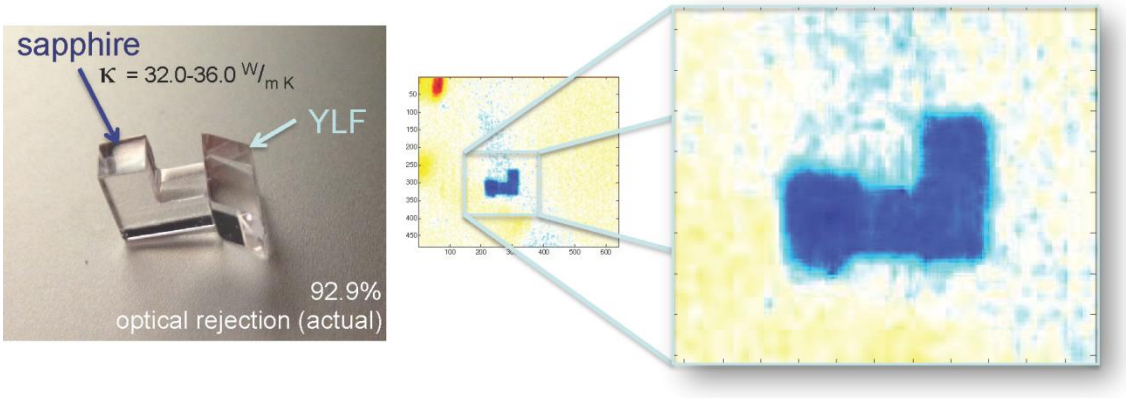

Fig. 16. Photograph of sapphire thermal link bonded to a 10% Yb:YLF crystal. Optical rejection of the link is measured at 92.9%. Thermal images: Cooling can be seen in the crystal and thermal link, which have been false colored as blue. No strong thermal discontinuity or thermal barrier is seen within the resolution of the thermal camera.

A significant improvement in thermal properties is measured for the sapphire thermal link, Fig. 16 compared to the fused silica link, Fig. 15. When measured quantitatively, Fig. 17, it can be seen that no thermal barrier exists for the Van Der Waals bonded sapphire link, while adhesive imposes significant impedance. Additionally, no thermal gradient exists along the length of the sapphire link, thanks to the high thermal conductivity, whereas the fused silica link exhibits a significant gradient.

It should be noted that thermal reflections from the lab environment can generate errors in the thermal image for sapphire. Even though the errors are reduced, a slight bump in the thermal image is detected due to a reflection from the mount, and could not be completely removed. Instead the reflection was placed at a portion of the link where it can be reasonably omitted, since it should be understood that the link end cannot be physically colder than the portion nearest the crystal, and therefore the link is uniformly cold.

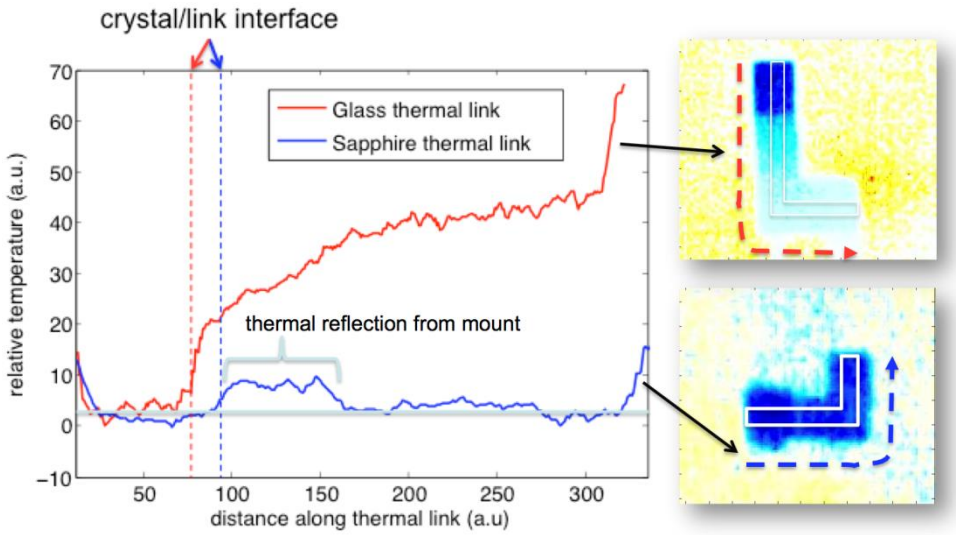

Fig. 17. Thermal profile of the fused silica (red) and sapphire link (blue).

Publications:

D. V. Seletskiy, S. D. Melgaard, R. I. Epstein, A. Di Lieto, M. Tonelli, and M. Sheik-Bahae, "Local laser cooling of Yb:YLF to 110 K," Optics Express, Vol. 19, pp. 18229-18236 (2011).

DV Seletskiy, MP Hehlen, RI Epstein, and M Sheik-Bahae, "Cryogenic optical refrigeration," Advances in Optics and Photonics 4 (1), 78-107 (2012).

Alexander R. Albrecht, Denis V. Seletskiy, Jeffrey G. Cederberg, Alberto Di Lieto, Mauro Tonelli, Jerome V. Moloney, Ganesh Balakrishnan, and Mansoor Sheik-Bahae, "Intracavity laser cooling using a VECSEL," Proc. SPIE 8275, Laser Refrigeration of Solids V, 827505 (February 9, 2012).

Mansoor Sheik-Bahae, Mohammad Ghasemkhani, Alexander R. Albrecht, Denis V. Seletskiy, Jeffrey G. Cederberg, Seth D. Melgaard, "Intracavity-enhanced laser cooling of solids using high power VECSELs at 1020 nm," Proc. SPIE 8606, Vertical External Cavity Surface Emitting Lasers (VECSELs) III, 86060A (February 26, 2013).

Chengao Wang, Mansoor Sheik-Bahae, Jeffrey Cederberg, and Daniel Bender, "Accurate measurement of external quantum efficiency in semiconductors," Proc. SPIE 8638, Laser Refrigeration of Solids VI, 86380H (March 11, 2013).

Alexander R. Albrecht, Mohammadreza Ghasemkhani, Jeffrey G. Cederberg, Denis V. Seletskiy, Seth D. Melgaard, Mansoor Sheik-Bahae, "Progress towards cryogenic temperatures in intra-cavity optical refrigeration using a VECSEL," Proc. SPIE 8638, Laser Refrigeration of Solids VI, 863805 (March 11, 2013).

D. V Seletskiy, S. D. Melgaard, R. I. Epstein, A. Di Lieto, M. Tonelli, and M. Sheik-Bahae, "Precise determination of minimum achievable temperature for solid-state optical refrigeration," J. Lumin., vol. 133, pp. 5–9 (2013).

J. G. Cederberg, A. R. Albrecht, M. Ghasemkhani, S. D. Melgaard, and M. Sheik-Bahae, "Growth and testing of vertical external cavity surface emitting lasers (VECSELs) for intracavity cooling of Yb:YLF," J. Cryst. Growth (2013), doi:10.1016/j.jcrysgro.2013.09.042.

Mohammadreza Ghasemkhani, Alexander R. Albrecht, Seth D. Melgaard, Denis V. Seletskiy, Jeffrey G. Cedeberg, Mansoor Sheik-Bahae, "Intracavity optical refrigeration to 131K using high-power vertical external-cavity surface-emitting lasers (VECSELs)," Proc. SPIE 9000, Laser Refrigeration of Solids VII, 900005 (February 19, 2014).

Seth D. Melgaard, Denis V. Seletskiy, Richard I. Epstein, Jay V. Alden, and Mansoor Sheik-Bahae, "Device applications of cryogenic optical refrigeration," Proc. SPIE 9000, Laser Refrigeration of Solids VII, 900002 (February 19, 2014).

Seth Melgaard, Denis Seletskiy, Victor Polyak, Yemane Asmerom, and Mansoor Sheik-Bahae, "Identification of Parasitic Losses in Yb:YLF and Prospects for Optical Refrigeration Down to 80K," Optics Express, Vol. 22, Issue 7, pp. 7756-7764 (2014)
http://www.opticsinfobase.org/oe/abstract.cfm?uri=oe-22-7-7756

Personnel working on this project:
Mansoor Sheik-Bahae, Prof. (PI)
Denis V. Seletskiy (NRC Postdoc Fellow)
Alexander R. Albrecht (postdoc)
Seth D. Melgaard (graduate student)
Mohammad Ghasemkhani (graduate student)